

Uptake of silver, gold, and hybrids silver-iron, gold-iron and silver-gold aminolevulinic acid nanoparticles by MCF-7 breast cancer cells

Karina de Oliveira Gonçalves^a, Daniel Perez Vieira^b, Débora Levy^c, Sergio Paulo Bydlowski^c, Lilia Coronato Courrol^{a,*}

^a Institute of Environmental, Chemical and Pharmaceutical Sciences, Department of Physics, Federal University of Sao Paulo, Diadema, Sao Paulo, Brazil

^b Biotechnology Center, Institute for Energy and Nuclear Research, Sao Paulo, SP, Brazil

^c Histocompatibility and Cellular Immunity Laboratory - LIM19, University of São Paulo School of Medicine SP, Brazil

ARTICLE INFO

Keywords:

Gold nanoparticles
Silver nanoparticles
Drug delivery
Photoreduction
Cancer
Photodynamic therapy

ABSTRACT

Background: Nanoparticles show promise for theranostic applications in cancer. The metal-based nanoparticles can be used both as photosensitizers and delivery vehicles. In bimetallic particles based on gold or silver and iron, a combination of the plasmonic features of the gold or silver components with the magnetic properties of the iron makes these hybrid nanomaterials suitable for both imaging and therapeutic applications. Herein, we discuss toxicity and cell internalization of metallic (silver and gold) and bimetallic (silver-iron, gold-iron, and silver-gold) aminolevulinic acid (ALA) nanoparticles. ALA can control the production of an intracellular photosensitizer, protoporphyrin IX (PpIX), commonly used in photodynamic therapy.

Methods: Nanoparticles were synthesized by photoreduction method and characterized by UV/Vis spectra, Zeta potential, FTIR, XRD, and transmission electron microscopy. The amount of singlet oxygen generation by a yellow LED, and ultrasound was studied for gold, gold-iron, and silver-gold nanoparticles. Cytotoxicity assays of MCF-7 in the presence of nanoparticles were performed, and PpIX fluorescence was quantified by high content screening (HCS).

Results: Red fluorescence observed after 24 h of nanoparticles incubation on MCF-7 cells, indicated that the ALA in surface of nanoparticles was efficiently converted to PpIX. The best results for singlet oxygen generation with LED or ultrasound irradiation were obtained with ALA:AgAuNPs.

Conclusions: The studied nanoparticles present the potential to deliver aminolevulinic acid to breast cancer cells efficiently, generate singlet oxygen, and convert ALA into PpIX inside the cells allowing photodiagnosis and therapies such as photodynamic and sonodynamic therapies.

1. Introduction

Breast cancer is one of the most critical malignancies in women, along with a significant cause of mortality worldwide [1]. Uncontrolled growth and metastasis to sites such as the brain, liver, and bone occur in 10 % of initial cases and can occur in 40 % in advanced stages [2].

In breast cancer treatment, the chemotherapeutic is one of the main therapeutic approaches. The major problem in chemotherapy is to deliver the drug to a specific place while avoiding toxicity and side effects in healthy cells [3]. Novel methods to improve the therapeutic index of chemotherapy are underway [4,5]. One possible strategy is the use of nanoparticulate colloidal systems [4].

Metal nanoparticles are attractive nanomaterials for biomedical

applications due to their physicochemical properties, easy conjugation with different biomolecules, and high surface reactivity [6,7].

Nanoparticles serve as efficient carriers improving the drug delivery to the tumor [8,9]. Besides the delivery of drugs to kill the tumor cells, the nanoparticles can cause the production of reactive oxygen species (ROS), changes in the cell cycle, damage to the genetic material, inflammatory processes, and cell death [10]. Generation of ROS induces apoptosis in various cell culture models [11]. With the delivery of the drug, it is also possible to perform therapies such as laser-induced hyperthermia [12], photodynamic therapy (PDT) [13], and sonodynamic therapy (SDT) [14]. PDT and SDT are treatment modalities that eradicate malignant tumors with the combination of light and a photosensitizer or ultrasound and sonosensitizer, respectively, and oxygen

* Corresponding author.

E-mail address: lcourrol@unifesp.br (L.C. Courrol).

<https://doi.org/10.1016/j.pdpdt.2020.102080>

Received 8 July 2020; Received in revised form 13 August 2020; Accepted 23 October 2020

Available online 4 November 2020

1572-1000/© 2020 Elsevier B.V. All rights reserved.

[15–17]. Aminolevulinic acid (ALA) is the natural precursor of protoporphyrin IX (PpIX), photo, or sonosensitizer used in PDT and SDT [18]. PpIX can accumulate in rapidly proliferating cells, such as tumors, compared to healthy cells. Exogenous ALA administration promotes selective tumor specificity for PDT and SDT [13]. Metallic or bimetallic nanoparticles can deliver ALA, improving penetration in the tissues and membranes. [19].

Some previous reports indicated the good quality of metallic nanoparticles synthesized with ALA and photoreduction method [16,20–24].

Bimetallic particles based on gold or silver and iron have been presented increasing interest due to the combination of the plasmonic features of the gold or silver components with the magnetic properties of the iron, which makes these hybrid nanomaterials suitable for imaging and therapeutic applications [23,25,26].

In this work, the breast cancer cell line MCF-7 internalization was studied employing the synthesized silver (Ag), gold (Au), and the hybrids silver-iron (Ag-Fe), gold-iron (Au-Fe) and silver-gold (Ag-Au) nanoparticles synthesized with ALA by photoreduction. Singlet oxygen generation was studied using a yellow LED and ultrasound. Cytotoxicity studies were performed with MCF-7 breast tumor cell. The cell internalization and the amount of PpIX after exposure to the nanoparticles was quantified by high content screening.

2. Materials and methods

2.1. Ag, Au, Ag-Fe, Au-Fe and Ag-Au with ALA synthesis

To prepare the ALA:AgNPs, 1 mmol of AgNO₃ were mixed with 0.3 mmol of ALA and 0.01 mmol of polyethylene glycol (PEG) in 100 mL of distilled water at 20 °C. The procedure was followed by vigorous stirring for 5 min, and 10 mL of the resulting solution was exposed to a 300 W Cermax Xenon lamp for 2 min.

For the synthesis of ALA:AuNPs, 0.3 mmol of ALA, 1 mmol of HAuCl₄ and 0.01 mmol of PEG were diluted in 100 mL of distilled water and followed by vigorous stirring for 5 min. After a solution (10 mL) was illuminated for 2 min.

For the synthesis of hybrids particles (gold-iron and silver-iron), 45 mg of iron powder was added to 100 mL of MilliQ water, and the pH was adjusted to ~12 using NaOH solution. Then the ALA (0.3 mmol), PEG (0.01 mmol), and AgNO₃ (1 mmol) or HAuCl₄ (1 mmol) and were added to the solution and illuminated for 2 min.

To prepare Ag-AuNPs, 1 mmol of AgNO₃ were mixed with 1 mmol of HAuCl₄ and 0.01 mmol of PEG in 30 mL of Milli-Q water and illuminated for 2 min.

All solutions have the pH solution adjusted to 7.0 after irradiation.

2.2. Nanoparticles characterization

The UV–vis absorption spectra were measured by a Shimadzu spectrophotometer, using 1-cm quartz cells.

The shape and sizes of Ag, Au, Ag-Fe, Au-Fe, and Ag-Au were obtained from transmission electron microscope (TEM) Joel (Zeiss, Germany) and image J analysis, respectively.

The surface charges on the nanoparticles were measured using Zeta potential (Malvern Instruments Zetasizer, Worcestershire, UK) and DKSH ZetaView.

The FTIR spectra were obtained in a Shimadzu Prestige-21 spectrometer (Shimadzu Corp., Kyoto, JP) with 2 cm⁻¹ resolution in the range of 4000 cm⁻¹ to 400 cm⁻¹.

The structural identification of the 5-ALA:AgFeNPs sample was performed by x-ray diffraction (XRD) measurement using a Bruker D8 Advance 3 kW diffractometer, with copper radiation tube. For this measurement, the silver-iron solution was submitted to a first magnetic separation using a magnet. Then, the supernatant was centrifuged for 5 min at 10,000 rpm, always separating the supernatant from the bottom body, and centrifuging the supernatant again. The process was repeated

five times, and the obtained content was dried in a greenhouse (60 °C) for 48 h.

2.3. Cell culture

The breast tumor cells MCF-7 were kept in RPMI 1640 medium supplemented with 10 % fetal bovine serum (FBS) and 1% penicillin/streptomycin at 37 °C with 5% CO₂. The cells were routinely subcultured every 3 days with 70–80 % confluency and harvested using 0.25 % trypsin.

2.4. Cell viability

The cells (8 × 10³ cells /well) were plated in the flat bottom 96 well plates and incubated for 24 h for plaque adhesion and growth. Then the plaque was divided into groups and incubated with ALA, ALA:AgNPs, ALA:AuNPs, ALA:AgFeNPs, ALA:AuFeNPs and ALA:AgAuNPs. The experimental groups received 50 µL of different dilutions (RPMI:NPs (µL), 45:5; 40:10; 30:20; 20:30 and 10:40).

The plates were then incubated for 24 h at 37 °C and 5% CO₂ atmosphere. Subsequently, the supernatant was removed, the cells were washed with PBS and incubated for 24 h in RPMI medium. Cell viability was evaluated by MTS (CellTiter 96® Aqueous MTS Reagent). The absorption band at 490 nm was directly proportional to the number of live cells in the culture. The results were statistically compared (ANOVA and Dunnett test) to negative (NaCl 0.9 %) or positive (latex powder suspension, 0.5 g/L filter sterilized latex extract, 0.5 g/L in culture media) controls. The percentage of cells survival was calculated after background absorbance correction and blank absorbance subtraction as follows:

$$\% \text{ Cell viability} = 100 \times \frac{\text{Experimental well absorbance}}{\text{untreated control well absorbance}}$$

2.5. PpIX fluorescence in flow-cytometry

MCF-7 cells (2 × 10⁵ cells/well) were plated in 6-well plates. After 24 h, the cells received 50 µL of 5-ALA:AuNPs and 2.5 mL of RPMI culture medium and were incubated in a greenhouse for 24 h. The cells were suspended with the use of Trypsin and centrifuged for 5 min at 1500 rpm. The supernatant was discarded, and the cells were resuspended in PBS. The material was analyzed in the flow cytometer (Accuri C6, BD Biosciences) with a laser at 488 nm, and filters FL1 (533/30 nm), FL2 (584/40 nm), FL3 (>670 nm) and FL4 (675/25 nm). Two measurements were made of each sample.

2.6. Quantification of PpIX fluorescence by high content screening (HCS)

The assay was performed in 96 well plates (Corning) with 2 × 10⁴ cells/well after 24 h of plating. An exchange of the culture medium was performed by the nanoparticle solution (10 µL of NPs in 40 µL of culture medium), which was then incubated for 24 h in an oven. After the exposure time, the cells were washed with PBS and one µL/well of the Hoechst 3342 fluorescence dye (1/100 dilution). Nine sites per well and three wells per treatment were acquired. The cells positive for PpIX fluorescence were determined using the cell scoring MetaXpress software.

2.7. Indirect release of singlet oxygen

Singlet oxygen (¹O₂) generation by nanoparticles was evaluated by monitoring the photoabsorption spectral change of the known ¹O₂ scavenger 1,3-diphenylisobenzofuran (DPBF). DPBF can trap ¹O₂ through its photooxidation. In a cuvette 10 µL of DPBF (diluted with

DMSO) was added to 1.0 mL of ALA:AuNPs, ALA:AuFeNPs or ALA:AuAgNPs. The photoabsorption spectral variation of DPBF with the irradiation or by light (Venus Sigma illumination system from MMOptics, Brazil, equipped with a LED at 590 ± 10 nm (InGaN) or by ultrasound (Sonic Compact, HTM, Brazil, 1 W/cm^2 and 1 MHz) was monitored with an interval of 1 min up to 10 min. The absorption band of DPBF (1,3-Diphenyl-isobenzofuran) at around 422 nm decreased with the increase in the irradiation time. The changes in optical density of DPBF are plotted against the light or ultrasound irradiation time, and the slope was used to estimate the quantity of singlet oxygen generated. No changes were observed in DPBF band with ALA and irradiation.

3. Statistical analysis

All studies were performed in triplicate. The results were statistically compared (ANOVA and Dunnett test) to controls.

4. Results and discussion

4.1. Nanoparticles characterization

The ALA:Ag and ALA:Au and hybrids ALA:AgFe, ALA:AuFe and ALA:AgAu nanoparticles were synthesized by the photoreduction method using a Xenon lamp.

The absorbance spectra of the ALA, ALA:AgNPs, and ALA:AuNPs solutions are shown in Fig. 1. Aminolevulinic acid exhibits the characteristic absorbance peak at 267 nm. The ALA:AgNPs solution presented the SPR (surface plasmon resonance) peak at 420 nm, indicating the presence of silver nanoparticles, whereas ALA:AuNPs solution presented the band characteristic present at ~ 522 nm. Fig. 1 shows the images of solutions before and after irradiation, indicating the change of color due to the presence of silver and gold nanoparticles.

Fig. 2 shows the absorbance results for the hybrids, ALA:AgFeNPs, ALA:AuFeNPs and ALA:AgAuNPs solutions produced with 2 min of Xenon illumination. It is possible to observe the silver SPR peak around 422 nm for AgFeNPs, and the gold SPR peak ~ 516 nm for AuFeNPs, and broad spectra with a maximum at ~ 557 nm for AgAuNPs.

Table 1 presents the obtained values of size, Zeta potential, and polydispersity index for the synthesized nanoparticles. The zeta potential is predominantly negative. Silver nanoparticles present higher stability (> -36 mV) than gold nanoparticles (~ -27 mV). The polydispersity index obtained for most of the nanoparticles around 0.4 indicate the good distribution of particles. The PDI value found to ALA:AgFeNPs, around 0.7, indicates that the sample has a very broad size distribution of aggregates.

The size and shape of the nanoparticles were obtained by

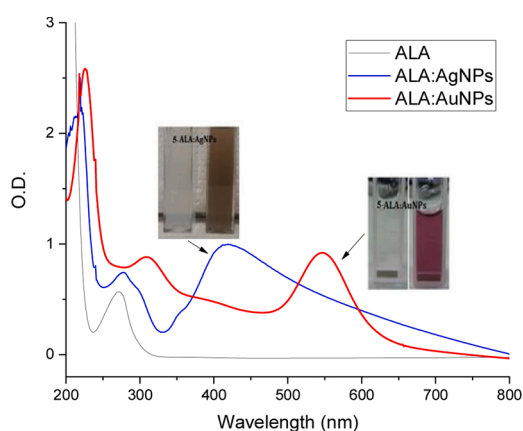


Fig. 1. Absorption spectra: ALA and ALA:AgNPs and ALA:AuNPs synthesized with 2 min of Xenon lamp exposure. The change in the solution color in both cases indicates the formation of the nanoparticles.

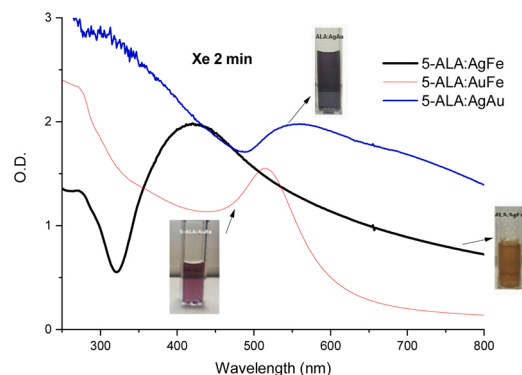


Fig. 2. UV-vis spectra: ALA:AgFeNPs ALA:AuFeNPs and ALA:AgAuNPs.

transmission electron microscopy (TEM) images shown in the Fig. 3a. It is possible to notice that ALA:AgNPs are quite heterogeneous, whereas ALA:AuNPs are spherical with low diversity of sizes. ALA:AgFeNPs and ALA:AuFeNPs presented, two sized nanoparticles, where larger particles were attributed to iron and the smallest to silver or gold. For the ALA:AgAuNPs, the presence of two sizes of nanoparticles was also observed. The distribution of the particle size evaluated by dynamic-light scattering are shown in Fig. 3b.

As the magnetism is associated with the formation of well-defined crystalline structures, XRD analyses were measured, and the result obtained for the ALA:AgFeNPs is showed in Fig. 4. The reflections referring to the interplanar distances characteristic of the crystalline phases of magnetite and silver can be observed. The diameter obtained for silver using Scherrer equation [27] was 12 nm, and for magnetite was 23 nm, which proves the results obtained by transmission electron microscopy, with smaller nanoparticles for silver and larger for iron.

The Fig. 5 shows the FTIR spectra obtained for ALA, ALA:AgNPs, ALA:AuNPs, ALA:AgFeNPs, ALA:AuFeNPs and ALA:AgAuNPs. The ALA presents lines corresponding to the OH/NH vibrations at $\sim 3500 \text{ cm}^{-1}$ and C=O vibrations at $\sim 1720 \text{ cm}^{-1}$ [28]. The Ag and Au and hybrids nanoparticles show bands in the same regions: $\sim 3432 \text{ cm}^{-1}$ (OH), $\sim 2880 \text{ cm}^{-1}$ (NH), 1720 cm^{-1} (C=O), and $\sim 1110 \text{ cm}^{-1}$ (C—O). The reduction of the intensity of C=O band, carboxyl ($\sim 1720 \text{ cm}^{-1}$), suggests strong interaction of the nanoparticles with this functional group. The band at 529 cm^{-1} appears in nanoparticles containing iron, which correspond to Fe—O bonds [29]. The band at 1376 cm^{-1} correspond to C—O stretch (phenolic) appears in nanoparticles containing silver. The bands at 688 and 465 cm^{-1} appear in nanoparticles containing gold, probably due to gold bonds.

4.2. Concentration of ALA:Au e ALA:Ag nanoparticles

The molar concentrations (c) of silver and gold nanoparticles were calculated using the formula [30]:

$$c = \frac{N_T}{NVN_A} \quad (3)$$

where N_T is the number of silver or gold atoms, N is the number of silver or gold atoms per nanoparticles, V is the volume of the colloidal suspension.

N was obtained by [30]:

$$N = \frac{\pi \rho d^3}{6M} N_A \quad (4)$$

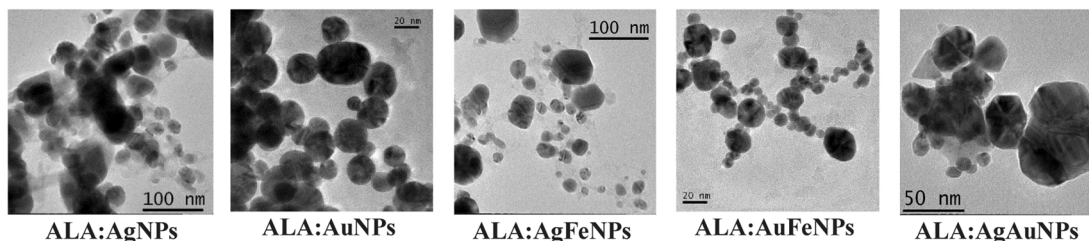
Where ρ is the density of face-centered cubic (fcc) silver (10.5 g/cm^3) or gold (19.6 g/cm^3), d is the average diameter of nanoparticle, M is the atomic mass of silver (107.87) or gold (196.97).

The obtained values were 8.61 nM for ALA:AgNPs and 55.5 nM for ALA:AuNPs.

Table 1
Size, Zeta potential, and polydispersity index of nanoparticles.

Parameter	ALA:AgNPs	ALA:AuNPs	ALA:AgFeNPs	ALA:AuFeNPs	ALA:AgAuNPs
Size (d. nm)	33.5 ± 3.48	18.12 ± 5.94	~12 and ~23	~18 and ~23	~30 and ~20
Zeta Potential (mV)	-36.6 ± 8.45	-27.1 ± 1.0	-37.9 ± 6.08	-29.0 ± 0.8	-37.9 ± 6.08
PDI	0.319	0.437	0.667	0.432	0.383
Hydrodynamic diameter (nm)	77.02	59.93	334.4 ± 0.84	75	77.0 ± 0.85
Absorbance peak (nm)	420	522	422	516	557

a)



b)

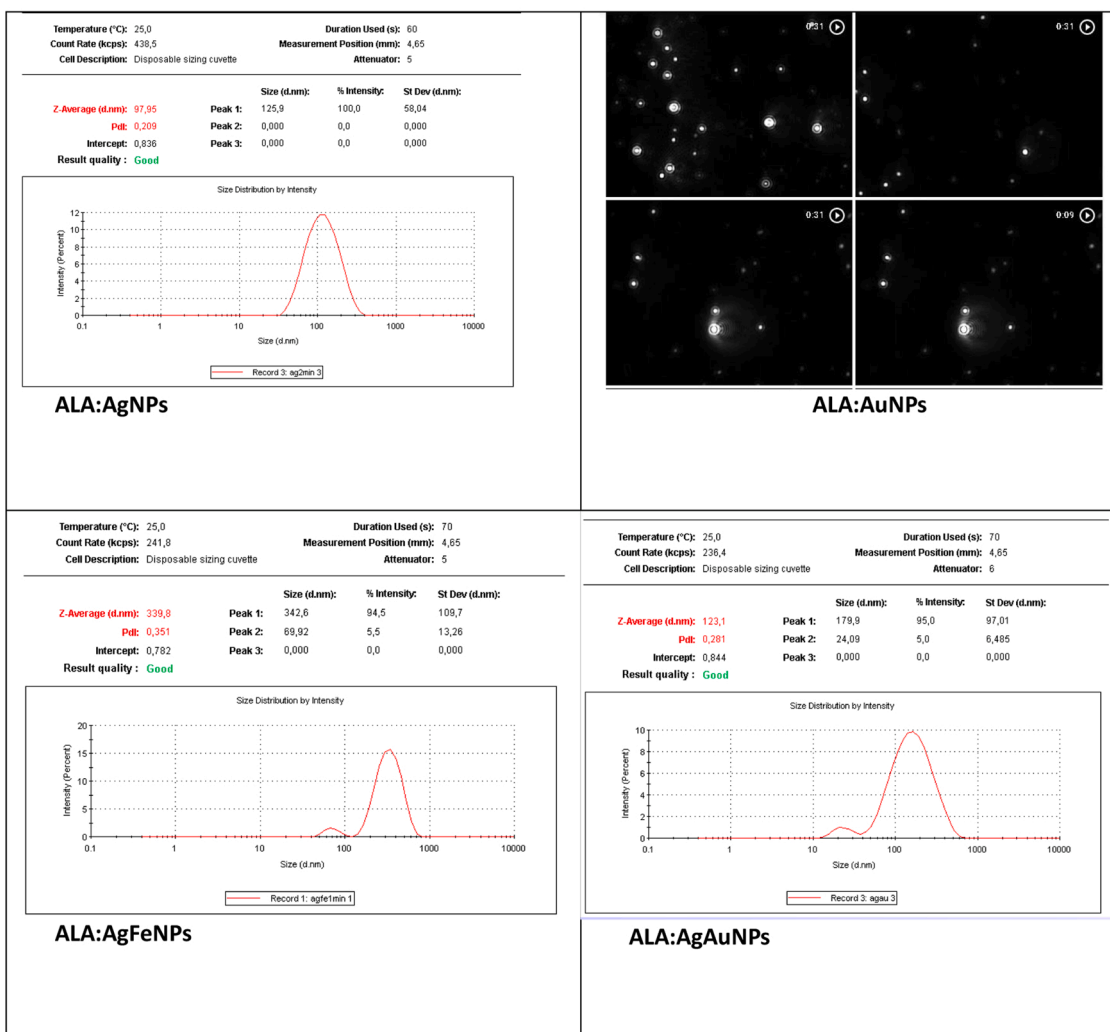


Fig. 3. a) TEM image of the samples. B) Size distribution for ALA:Ag, ALA:AgFe and ALA:AgAu nanoparticles and ZetaView light scattering for ALA:AuNPs. Each particle in the field of view of the camera is detected and tracked in its movement in a two-dimensional direction.

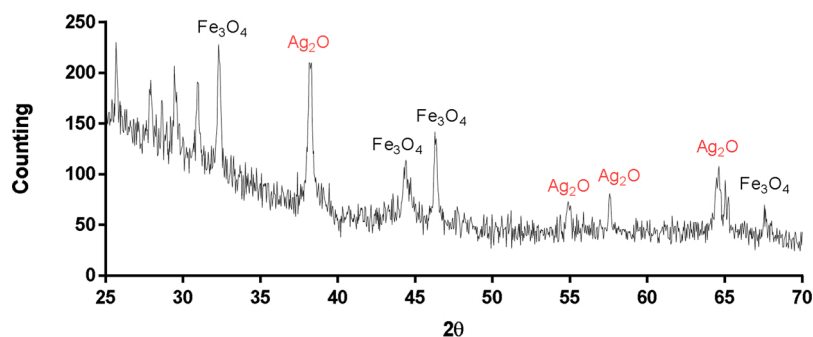


Fig. 4. Diffractogram of silver-iron core-satellite particles (5-ALA:AgFeNPs - 2 min of illumination - pH 7.2).

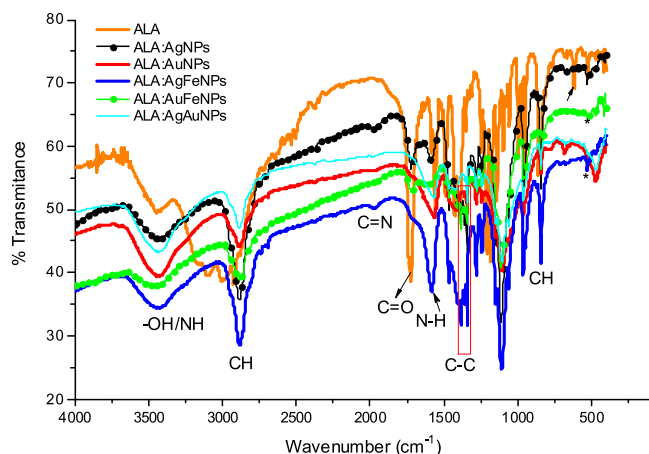


Fig. 5. FTIR spectra of the nanoparticles: spectrum of ALA, ALA:AgNPs, ALA:AuNPs, ALA:AgFeNPs, ALA:AuFeNPs and ALA:AgAuNPs.

4.3. Toxicity of nanoparticles

The cytotoxicity effects of ALA, ALA:AgNPs, ALA:AuNPs, ALA:AgFeNPs, ALA:AuFeNPs and ALA:AgAuNPs in MCF-7 cells can be observed in Fig. 6, where the percentage of cell viability is plotted in function of the volume of solution added in each well.

As observed in Fig. 6, ALA (10 μ L) did not produce any cytotoxic effect in the cells, and the percentage of viable cells was the same as the control group CC. ALA:AgNPs did not present high toxicity at low concentrations of solution (5 and 10 μ L). ALA:AgFeNPs were more toxic than ALA:AgNPs.

The calculated values of the LD50 (Lethal Dose 50 %), dose at which 50 % of the MCF-7 cells will be expected to die, for silver and gold nanoparticles were found \sim 29.65 μ L or 2.37 nM and \sim 0.75 μ L or 0.4 nM, respectively.

4.4. PpIX fluorescence

4.4.1. Flow cytometry

Analysis of the PpIX fluorescence done by flow cytometry for MCF-7 (control) and MCF-7 cells incubated with ALA:AuNPs are shown in Fig. 7a and b, respectively. Filters used were FL1 (533/30 nm), FL2 (584/40 nm), FL3 ($>$ 670 nm), and FL4 (675/25 nm). The control group presented fluorescence for the filters FL1, 2, and 3. The data show a shift in the positive area for cell lines incubated with ALA:AuNPs compared with control cells. For the FL4 filter, the protoporphyrin IX fluorescence signal (from 580 to 750 nm) was observed in the cells incubated with nanoparticles.

4.4.2. High content screening

The control group and the groups of the nanoparticles were analyzed by high content screening. Quantitation of labeled cell emitters of PpIX fluorescence was done. The data are shown in Fig. 8a and b for cells incubated with nanoparticles by 4 and 24 h, respectively. The blue color represents the viable cells and the red color, the PpIX fluorescence, due to the conversion of ALA into PpIX.

The percentage of cells labeled with PpIX is shown in Fig. 9 by nanoparticles incubated for 4 and 24 h. The experimental groups of ALA: NPs show significance when compared to the control group (CC). This result demonstrates that nanoparticles entered in the cells carrying ALA. The ALA:AuNPs and ALA:AgNPs groups presented \sim 50 % and \sim 13 % labeled cells, respectively, after 24 h of incubation. The PpIX concentration observed in cells incubated with ALA:AuNPs for 24 h was higher than cells incubated with ALA. The conversion to PpIX was slower for cells incubated with nanoparticles.

4.5. Indirect release of singlet oxygen with LED and ultrasound

Fig. 10 shows the UV-vis spectra of ALA:AuNPs, ALA:AuFeNPs, and ALA:AgAuNPs in the presence of DPBF, measured in function of the time of LED (a, b, c) and ultrasound irradiation (d, e, f). The DPBF absorption intensity around 420 nm decreases with the incidence of irradiation, indicating the generation of singlet oxygen. The band around 520 nm, characteristic of SPR peak of gold nanoparticles, remains practically unchanged until 10 min of irradiation.

Using the Beer Law (Eq.1), the molar absorbance value (ϵ) of the DPBF was calculated ($\epsilon_{DPBF} = 2375 \text{ L/mol.cm}$). The consumption of DPBF as a function of irradiation time (Eq.1) and quantity of $^1\text{O}_2$ generated by irradiation was calculated according to (Eq.2).

$$A = \epsilon \cdot b \cdot c \quad (1)$$

$$[^1\text{O}_2]_t = [\text{DPBF}]_0 - [\text{DPBF}]_t = (A_0 / \epsilon \text{ DPBF}) - (A_t / \epsilon \text{ DPBF}) \quad (2)$$

Table 2 shows the results obtained from the consumption of the DPBF reagent by time and generation from $^1\text{O}_2$ with LED or ultrasound irradiation. The results show that the presence of iron inhibits the $^1\text{O}_2$ liberation in the case of LED irradiation, and the highest values of singlet oxygen liberation were obtained for ALA:AgAuNPs with 8 min of LED ultrasound irradiation. Ultrasound irradiation demonstrated a high ability to generate $^1\text{O}_2$. These results prove the ability of nanoparticles to produce reactive oxygen species in aqueous solutions.

5. Discussion

ALA nanoparticles were synthesized by photoreduction [31,32]. This method is eco-friendly, clean, and has great versatility. The light properties allow the control of the photochemical reactions facilitating silver and gold salts reduction. The light irradiation acted as a catalyst for the metal reduction Ag^+ into Ag^0 and Au^{3+} into Au^0 . Aminolevulinic acid, present in the solution, acts as a capping agent and inhibits the ions

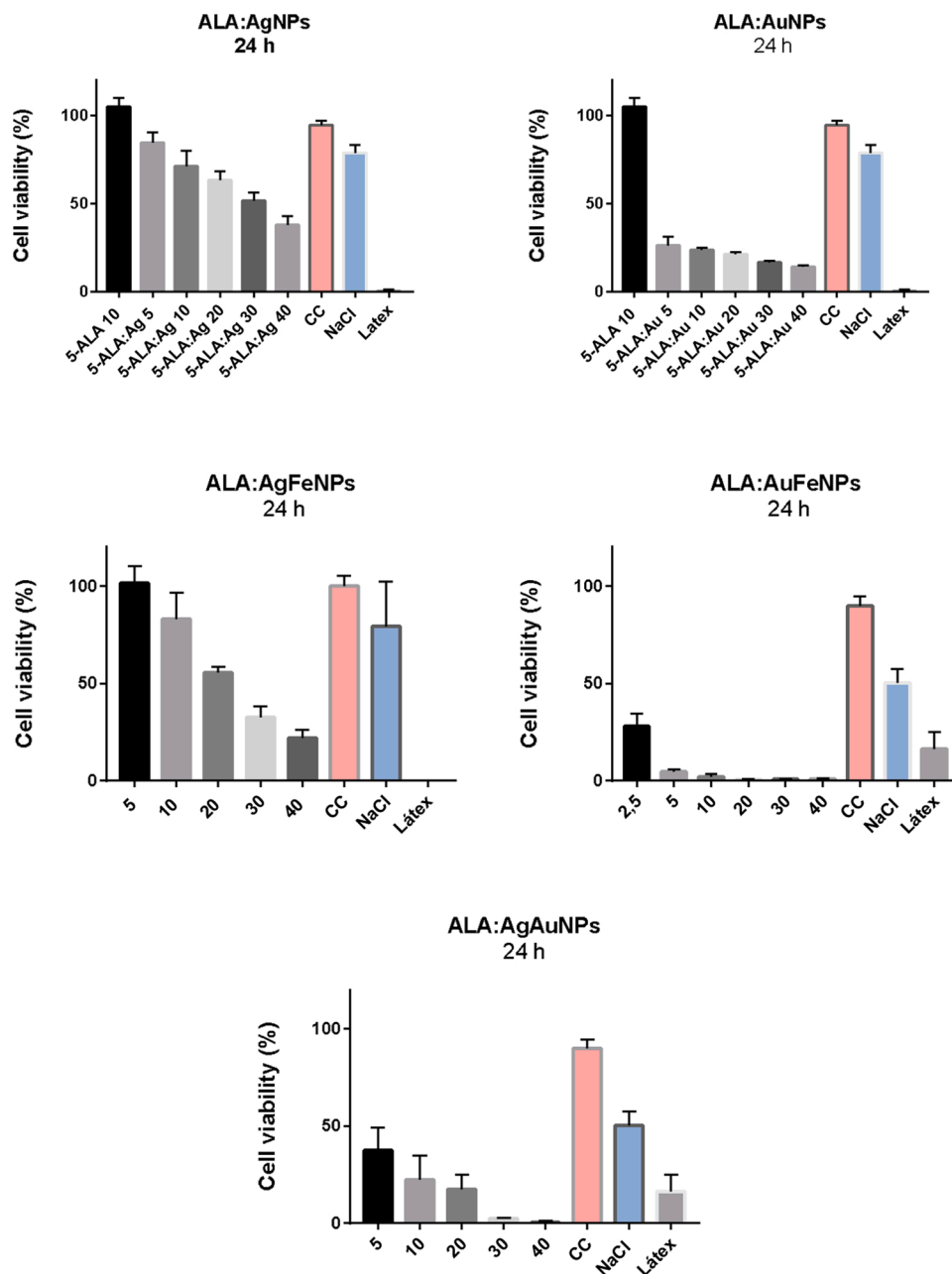


Fig. 6. Cell viability test in MCF-7 lineage, incubated for 24 h with ALA, ALA:AgNPs, ALA:AuNPs, ALA:AgFeNPs, ALA:AuFeNPs and ALA:AgAuNPs in different dilutions (RPMI:NPs (μ L), 45:5; 40:10; 30:20; 20:30 and 10:40). Data were compared using the ANOVA test followed by the Dunnett test, with $p < 0.0001$.

agglomerations to produce nanoparticles.

The light promotes iron oxidation in water solution and the photochemical reduction of ferric iron Fe(III) to ferrous iron Fe(II). The XRD analysis indicated the formation of crystalline structured iron oxides like magnetite (Fig. 4). The hybrids Ag-Fe and Au-Fe nanoparticle images indicate that iron nanoparticles are distributed around the silver or gold (Fig. 5).

Following the successful synthesis of silver, gold, and hybrids nanoparticles, their uptakes into cancer cells were examined. ALA did not produce any cytotoxic effect on MCF-7 in the studied concentration. ALA:AgNPs did not present high toxicity at low concentrations of solution (5 and 10 μ L) and ALA:AgFeNPs were more toxic than ALA:AgNPs (Fig. 6). ALA:AuNPs, were very toxic to the cells producing more than 50 % of cell death. ALA:AuFeNPs were more toxic to the cells than ALA:AgAuNPs.

The results demonstrated that the presence of Fe₃O₄ nanoparticles

increased the toxicity effect of silver and gold nanoparticles. The distribution of electronic or ion chains in the cell membrane resulted in a strong affinity of nanoparticles, which may block transcriptional regulation and protein synthesis resulting in cell death. [33]

The PpIX fluorescence of cells incubated with ALA:AuNPs was observed by flow cytometry. The gold nanoparticles loaded cells accumulating in S-phase, indicating that cells were arrested due to DNA damage (Fig. 7b).

The presence of nanoparticles inside cells is proved by the presence of PpIX emission observed in HCS. Hoechst staining assay was performed to detect the viable cell incubated with nanoparticles by confocal laser scanning microscopy (Fig. 8). The uptake and conversion of ALA into PpIX inside the cells were observed. For the control group, the nuclei were stained into blue, and no red emission appeared in the image. In the presence of nanoparticles, the cell numbers reduced, and some cells presented red emission due to the conversion ALA-PpIX. The

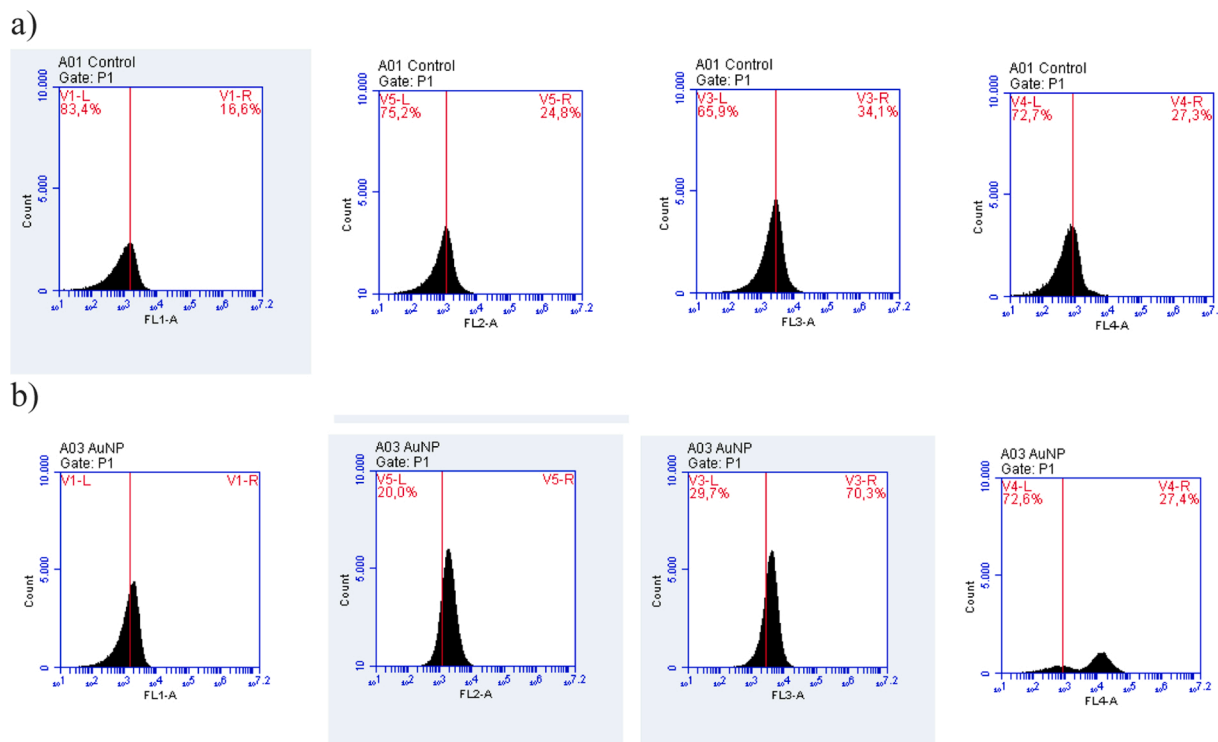


Fig. 7. a) Emission spectra obtained by flow cytometry for the Control group. Peaks correspond to the event count (cells). b) Emission spectra obtained for the experimental group ALA:AuNPs. The FL4-A filter presents PpIX fluorescence at 674 nm.

changes in nuclei and cell morphology was also observed. Cells in the control groups preserves their shapes after 24 h. Comparing to the control group, cells exposed to the nanoparticles showed membrane instability and cytoskeleton disturbance. It is possible to observe a shrink margin loss of contact with the adjacent cells and the decrease in amount. With the increasing of incubating time, the cell nuclei must display typical apoptosis characteristics, such as fragmentation, condensed chromatin, and reduction of cellular volume, but from the images, it is not easy to identify chromatin aggregation [5].

The images obtained for MCF-7 cells incubated with ALA:AgNPs for 4 h show that cells are separated one from the other. A repulsive force pushes the cells apart. A negatively charged cell exerts a repulsive force upon a second negatively charged cell. The measured Zeta potential was around -27 mV for gold and gold-iron nanoparticles and around -38 mV for silver and silver-iron and silver-gold nanoparticles. Zhang et al. measured the Zeta potential for MCF-7 cells as -20.32 ± 2.43 mV and demonstrated that the internalization process resulting in the change of Zeta potential due to the vesicular transport-based cell endocytosis [34]. Since the prepared nanoparticles are all negatively charged on the surface, electrostatic repulsion between anionic nanoparticles and negatively charged cell membrane should repel the uptake of nanoparticles. The Zeta potential of MCF-7 cells should become more negative after incubated with nanoparticles, which might be due to the dominant binding effect of nanoparticles on the cell surface membrane. If we compare the images obtained by HCS (Fig. 8a) for ALA:AgNPs and ALA:AgFeNPs, we observed a repulsive aspect for ALA:AgNPs with 4 h of incubation time, but not for ALA:AgFeNPs. AgNPs induce structural damage, accumulate in mitochondria, and contribute to oxidative stress [35]. The cytotoxic effects may be partially due to direct action of Ag⁺ ions released from AgNPs. The free Ag⁺ ions consequently may interfere with several cytoplasmic structures and pathways, including mitochondrial functions inducing stress pathways and apoptosis.

Specific proteins could mediate nevertheless the uptake of nanoparticles by cells despite their negative surface charge. Although silver nanoparticles have a much lower Zeta potential value, ~ -38 mV compared

to -30 mV of gold nanoparticles, after incubated with cells for longer time (24 h), nanoparticles should have adsorbed proteins on their surfaces and silver nanoparticles surface charge became close to the gold nanoparticles.

Several studies showed that porphyrins preferentially accumulate in tumors (pH \sim 6.9) compared to healthy cells (pH \sim 7.4). The accumulation of PpIX in cancer cells is affected by multiple biological factors, including transporters that mediate the uptake of ALA into cells and excrete PpIX from cells, enzymes, especially ferrochelatase, and the intracellular Fe²⁺ content. PpIX is synthesized in mitochondria from ALA by heme synthesis enzymes. Hagiya et al. demonstrated that the balance between ALA uptake and PpIX excretion was a substantial factor that determines the intracellular accumulation of PpIX [36]. The accumulation of PpIX in MCF-7 cells is related to the balance between the generation of PpIX from ALA in cells and the excretion of PpIX outside the cell [37]. Our results suggest that cells can incorporate ALA and metabolize ALA to generate PpIX. Li et al. observed that PpIX mostly accumulated in the mitochondria of MCF-7 [38]. PpIX accumulated in the mitochondria have a great influence on subsequent cell damage, and oxidative stress might be one of the significant causes that initiate cell death since PpIX accumulation induces DNA damage in MCF-7 [38].

ROS are generally considered cytotoxic since the radicals can provide oxidative damage to biomolecules such as DNA, proteins, and lipids. The production of ¹O₂ concerning the other ROS becomes an important differential, since the ¹O₂ has a limited lifetime, and when returning to its fundamental state, it automatically loses its reactivity. We observe ¹O₂ generation for ALA:Au, ALA:AuFe, ALA:AgFe and ALA:AgAu where excited by light at 590 nm or ultrasound. Irradiation of gold nanoparticles at 590 nm leads to the excitation of their plasmon resonance, which can be described as a coherent oscillatory motion of the conduction band electrons. The excited electrons initially have a nonthermal energy distribution, and the interaction with other electrons by electron-electron scattering to yield of Fermi distribution has their temperature increased. The "hot electrons" can dissociate gold-ALA bonds at the surface of gold nanoparticles and are responsible for the

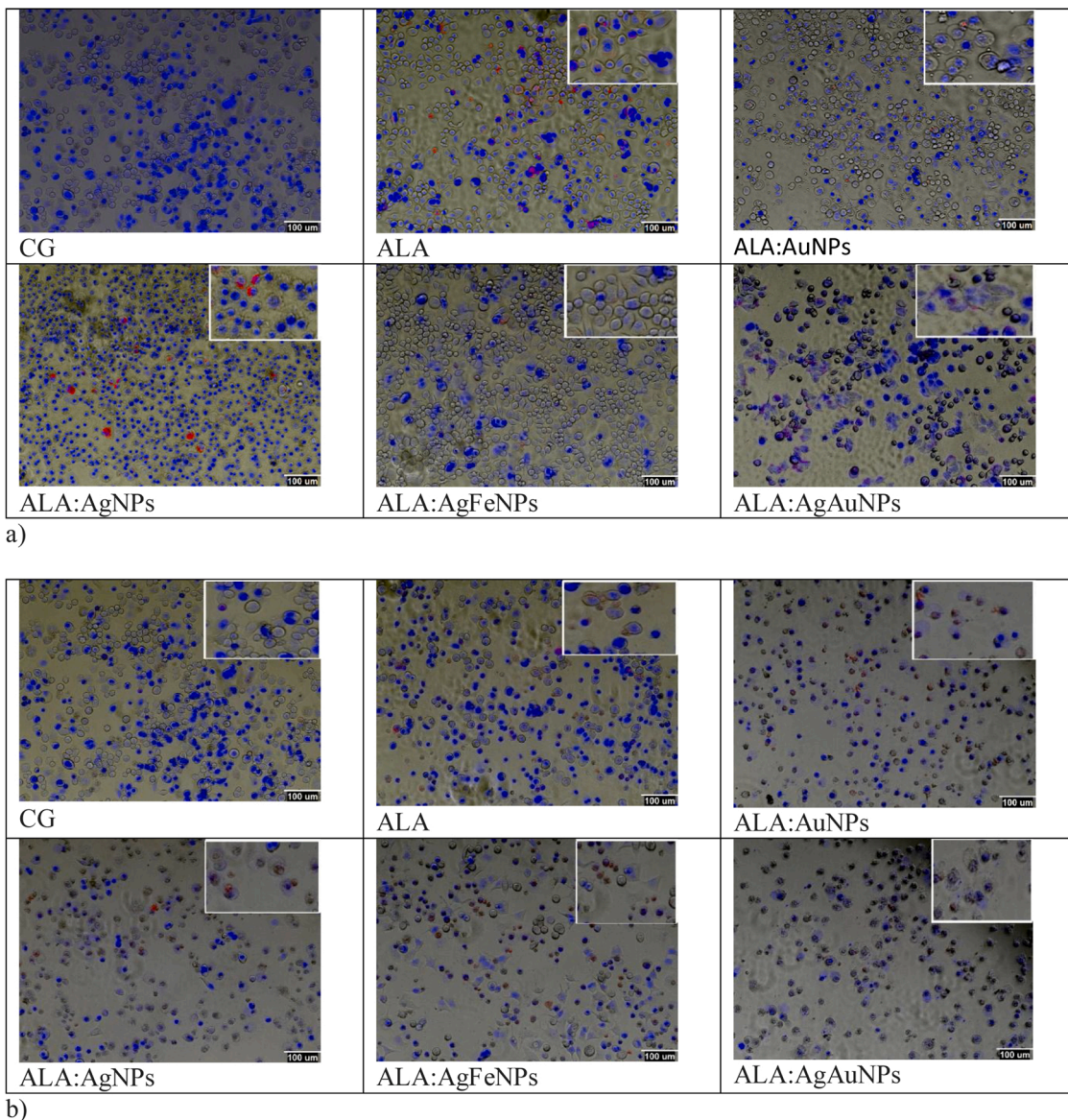


Fig. 8. MCF-7 cells incubated with nanoparticles: control group (cells), ALA, ALA:AgNPs, ALA:AuNPs, ALA:AgFeNPs ALA:AgAuNPs for a) 4 h and b) 24 h. The cells were stained with Hoechst 3342, 2 h before the images were obtained.

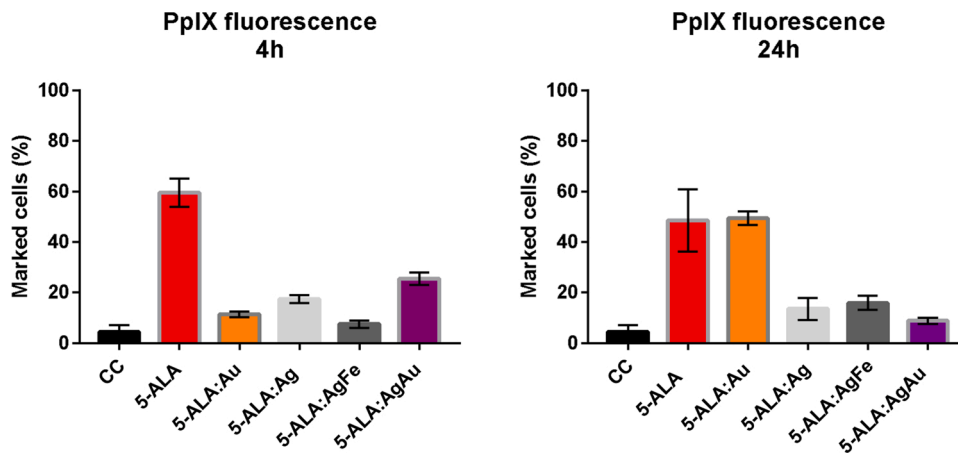


Fig. 9. PpIX fluorescence (675 nm) of cells incubated for 24 h with ALA, ALA:AuNPs, ALA:AgNPs, ALA:AgFeNPs and ALA:AgAuNPs for 4 and 24 h. The cells were stained with Hoechst 3342 2 h before the images were obtained. In the "a" plot, the data were compared using the ANOVA test followed by the Dunnet test, with p-value: **** < 0.0001.

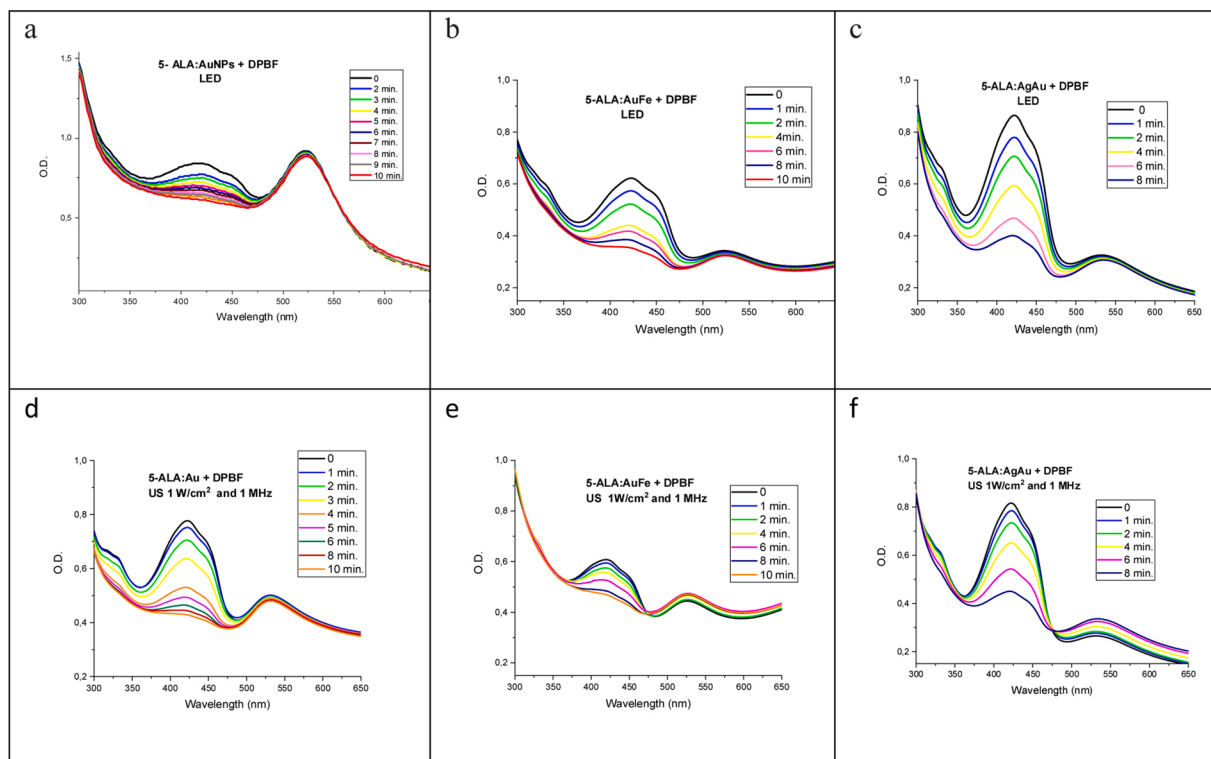


Fig. 10. Profile of the photodegradation of DPBF (420 nm) by irradiation with LED (a, b, c) and ultrasound (d, e, f) for ALA:AuNPs, ALA:AuFeNPs, and ALA:AgAuNPs.

Table 2

Release of singlet oxygen by nanoparticles after exposure to LED at different times.

Nanoparticles	Singlet oxygen (mmol/L)					
	LED 2 min.	LED 4 min.	LED 8 min.	US 2 min.	US 4 min.	US 8 min.
5-ALA:AuNPs	1.150	1.452	1.753	0.494	1.231	1.590
5-ALA:AuFeNPs	0.425	0.862	0.999	0.082	0.119	0.181
5-ALA:AgAuNPs	0.651	1.656	1.942	0.211	0.458	0.506

generation of $^1\text{O}_2$ by irradiation of gold nanoparticles [39].

The ultrasonic waves cause thermal and non-thermal effects. An increase in temperature due to the absorption of the ultrasonic waves creates mechanical compression and decompression. The non-thermal effect comprising stable and inertial cavitation, and radiation forces able to induce both temperature increase and mechanical stresses [40]. The inertial cavitation can induce water thermal dissociation and, thus, reactive oxygen species (ROS). A synergistic effect of Fe_3O_4 nanoparticles with low-intensity ultrasound enhances the release of iron, necessary to trigger the Fenton reaction, responsible for the ROS generation [41].

Using ALA nanoparticles as photo or sonosensitizers, singlet oxygen generation can occur through the transfer of energy from the triplet state of PpIX to molecular oxygen, leading to the type II reaction. Generation of excessive intracellular ROS leads to apoptosis and necrosis [35], evidenced by the fact that an increase in ROS levels is correlated with massive DNA breakage and high levels of apoptosis and necrosis [42].

In the present study, PDT or SDT therapies were not necessary for the apoptosis of MCF7 cells as the nanoparticles in themselves were very toxic. However, the toxic response varies depending on the type of cell exposed since the cellular response not to be identical, depending on the cell death mechanism [16,43] and, in some cases, the SDT and PDT associated with the ALA nanoparticles is the key in treatment.

6. Conclusions

In summary, we report the synthesis of silver, gold, and bimetallic silver-iron, gold-iron, and silver-gold nanoparticles with ALA by the photoreduction method. ALA was incorporated into the surface of the nanoparticles by the carboxyl functional group. Its internalization in MCF-7 cells was evaluated. The nanoparticles significantly enhanced the cytotoxicity of the cells comparing to ALA. Silver nanoparticles had a lower Zeta potential value of ~ -38 mV compared to -30 mV of gold nanoparticles. It was observed a repulsive aspect for ALA:AgNPs with 4 h of incubation time, but not for ALA:AgFeNPs. After incubated with cells for a longer time (24 h), nanoparticles should adsorb proteins on their surfaces, and silver nanoparticles surface charge became close to gold nanoparticles. Gold nanoparticles were more efficient in ALA conversion inside the cell and were more toxic than silver nanoparticles. The flow cytometry results showed that the gold nanoparticles could induce apoptosis and cell cycle S phase arrest.

Acknowledgments

The authors would like to thank Multiuser Centers of Universidade Federal do ABC (UFABC), Energy and Nuclear Research Institute (IPEN/CNEN-SP), The National Institute of Science and Technology Complex Fluids (INCT-FCX) grant 2014/50983-3 and São Paulo Research Foundation (FAPESP) grants 2014/06960-9 and 2017/23686-6.

References

- [1] O. Mandrik, N. Zielonke, F. Meheus, J.L. Severens, N. Guha, R.H. Acosta, R. Murillo, Systematic reviews as a 'lens of evidence': determinants of benefits and harms of breast cancer screening, *Int. J. Cancer* 145 (4) (2019) 994–1006.
- [2] A. Soni, Z. Ren, O. Hameed, D. Chanda, C.J. Morgan, G.P. Siegal, S. Wei, Breast cancer subtypes predispose the site of distant metastases, *Am. J. Clin. Pathol.* 143 (4) (2015) 471–478.
- [3] A.L. Demain, P. Vaishnav, Natural products for cancer chemotherapy, *Microb. Biotechnol.* 4 (6) (2011) 687–699.

- [4] H. Chen, X. Zhang, S. Dai, Y. Ma, S. Cui, S. Achilefu, Y. Gu, Multifunctional gold nanostar conjugates for tumor imaging and combined photothermal and chemotherapy, *Theranostics* 3 (9) (2013) 633–649.
- [5] R.W. Johnstone, A.A. Ruefli, S.W. Lowe, Apoptosis: a link between cancer genetics and chemotherapy, *Cell* 108 (2) (2002) 153–164.
- [6] R. Banerjee, A. Jaiswal, Recent advances in nanoparticle-based lateral flow immunoassay as a point-of-care diagnostic tool for infectious agents and diseases, *Analyst* 143 (9) (2018) 1970–1996.
- [7] H.A. Hemeg, Nanomaterials for alternative antibacterial therapy, *Int. J. Nanomed.* 12 (2017) 8211–8225.
- [8] N. Aich, J. Plazas-Tuttle, J.R. Lead, N.B. Saleh, A critical review of nanohybrids: synthesis, applications and environmental implications, *Environ. Chem.* 11 (6) (2014) 609–623.
- [9] H. Barabadi, M. Owais, Z.K. Shinwari, M. Saravanan, Anti-cancer green bionanomaterials: present status and future prospects, *Green Chem. Lett. Rev.* 10 (4) (2017) 285–314.
- [10] N. Elahi, M. Kamali, M.H. Baghersad, Recent biomedical applications of gold nanoparticles: a review, *Talanta* 184 (2018) 537–556.
- [11] L.A. Austin, S. Ahmad, B. Kang, K.R. Rommel, M. Mahmoud, M.E. Peek, M.A. El-Sayed, Cytotoxic effects of cytoplasmic-targeted and nuclear-targeted gold and silver nanoparticles in HSC-3 cells - a mechanistic study, *Toxicol. Vitro.* 29 (4) (2015) 694–705.
- [12] A. Ambrosone, P. del Pino, V. Marchesano, W.J. Parak, J.M. de la Fuente, C. Tortiglione, Gold nanoprisms for photothermal cell ablation in vivo, *Nanomedicine* 9 (13) (2014) 1913–1922.
- [13] A.P. Castano, T.N. Demidova, M.R. Hamblin, Mechanisms in photodynamic therapy: part one-photosensitizers, photochemistry and cellular localization, *Photodiagn. Photodyn. Ther.* 1 (4) (2004) 279–293.
- [14] D. Costley, C. Mc Ewan, C. Fowley, A.P. McHale, J. Atchison, N. Nomikou, J. F. Callan, Treating cancer with sonodynamic therapy: a review, *Int. J. Hyperth.* 31 (2) (2015) 107–117.
- [15] H. Abrahamse, M.R. Hamblin, New photosensitizers for photodynamic therapy, *Biochem. J.* 473 (2016) 347–364.
- [16] K.D. Goncalves, D.P. Vieira, L.C. Courrol, Synthesis and characterization of aminolevulinic acid gold nanoparticles: photo and sonosensitizer agent for atherosclerosis, *J. Lumin.* 197 (2018) 317–323.
- [17] Z.X. Zhang, S.J. Wang, H. Xu, B. Wang, C.P. Yao, Role of 5-aminolevulinic acid-conjugated gold nanoparticles for photodynamic therapy of cancer, *J. Biomed. Opt.* 20 (5) (2015) 8.
- [18] J.C. Kennedy, R.H. Pottier, Endogenous protoporphyrin-IX, a clinically useful photosensitizer for photodynamic therapy, *J. Photochem. Photobiol. B-Biol.* 14 (4) (1992) 275–292.
- [19] N. Fotinos, M.A. Campo, F. Popowycz, R. Gurny, N. Lange, 5-aminolevulinic acid derivatives in photomedicine: characteristics, application and perspectives, *Photochem. Photobiol.* 82 (4) (2006) 994–1015.
- [20] d.O. Goncalves Karina, N. da Silva Monica, C. Courrol Lilia, Identification of atherosclerosis using aminolevulinic gold nanoparticle assay in fecal specimens, in: C. Kurachi, K. Svanberg, B.J. Tromberg, V.S. Bagnato (Eds.), *Biophotonics South America*, 2015.
- [21] K.D. Goncalves, M.N. da Silva, L.B. Sicchieri, F.R.D. Silva, R.A. de Matos, L. C. Courrol, Aminolevulinic acid with gold nanoparticles: a novel theranostic agent for atherosclerosis, *Analyst* 140 (6) (2015) 1974–1980.
- [22] K.D. Goncalves, T.D. Cordeiro, F.R.D. Silva, R.E. Samad, N.D. Vieira, L.C. Courrol, Preparation and optimization of aminolevulinic acid with gold nanoparticles for photothermal and photodynamic therapies applications, in: C. Kurachi, K. Svanberg, B.J. Tromberg, V.S. Bagnato (Eds.), *Biophotonics South America*, 2015.
- [23] K.D. Goncalves, F.R.D. Silva, D.P. Vieira, L.C. Courrol, Ieee, Synthesis of Hybrid AuFe Nanoparticles by Photoreduction and Methyl Aminoluvinate, 2018.
- [24] D.G. Karina, N.D. Monica, L.C. Courrol, Identification of atherosclerosis using aminolevulinic gold nanoparticle assay in fecal specimens, in: C. Kurachi, K. Svanberg, B.J. Tromberg, V.S. Bagnato (Eds.), *Biophotonics South America*, 2015.
- [25] K.D. Gilroy, A. Ruditskiy, H.C. Peng, D. Qin, Y.N. Xia, Bimetallic nanocrystals: syntheses, properties, and applications, *Chem. Rev.* 116 (18) (2016) 10414–10472.
- [26] D.S. Sheny, J. Mathew, D. Philip, Phytosynthesis of Au, Ag and Au-Ag bimetallic nanoparticles using aqueous extract and dried leaf of *Anacardium occidentale*, *Spectrochim. Acta Part A-Mol. Biomol. Spectroscopy* 79 (1) (2011) 254–262.
- [27] H. Wang, X.Y. Qin, Z.Y. Li, Z.Z. Zheng, T.Y. Fan, [Preparation and characterization of citric acid-modified superparamagnetic iron oxide nanoparticles], *Beijing Da Xue Xue Bao* 50 (2) (2018) 340–346.
- [28] J.Y. Chen, Q. Peng, H.J. Jodl, Infrared spectral comparison of 5-aminolevulinic acid and its hexyl ester, *Spectrochim. Acta A. Mol. Biomol. Spectrosc.* 59 (11) (2003) 2571–2576.
- [29] G.S. Antipas, E. Statharas, P. Tserotas, N. Papadopoulos, E. Hristoforou, Experimental and first-principles characterization of functionalized magnetic nanoparticles, *Chemphyschem* 14 (9) (2013) 1934–1942.
- [30] X.O. Liu, M. Atwater, J.H. Wang, Q. Huo, Extinction coefficient of gold nanoparticles with different sizes and different capping ligands, *Colloids Surf. B-Biointerfaces* 58 (1) (2007) 3–7.
- [31] R. Bunsen, H.E. Roscoe, Photo-chemical Researches, Royal Society?, London?, 1857.
- [32] L.C. Courrol, F.R.D. Silva, L. Gomes, A simple method to synthesize silver nanoparticles by photoreduction, *Colloids Surf. A-Physicochem. Eng. Aspects* 305 (1–3) (2007) 54–57.
- [33] B. Ankamwar, T.C. Lai, J.H. Huang, R.S. Liu, M. Hsiao, C.H. Chen, Y.K. Hwu, Biocompatibility of Fe₃O₄ nanoparticles evaluated by in vitro cytotoxicity assays using normal, glia and breast cancer cells, *Nanotechnology* 21 (7) (2010).
- [34] M. Sakamoto, M. Fujistuka, T. Majima, Light as a construction tool of metal nanoparticles: synthesis and mechanism, *J. Photochem. Photobiol. C-Photochem. Rev.* 10 (1) (2009) 33–56.
- [35] P.V. AshaRani, G. Low Kah Mun, M.P. Hande, S. Valiyaveetil, Cytotoxicity and genotoxicity of silver nanoparticles in human cells, *ACS Nano* 3 (2) (2009) 279–290.
- [36] Y. Hagiya, Y. Endo, Y. Yonemura, K. Takahashi, M. Ishizuka, F. Abe, T. Tanaka, I. Okura, M. Nakajima, T. Ishikawa, S. Ogura, Pivotal roles of peptide transporter PEPT1 and ATP-binding cassette (ABC) transporter ABCG2 in 5-aminolevulinic acid (ALA)-based photocytotoxicity of gastric cancer cells in vitro, *Photodiagnosis Photodyn. Ther.* 9 (3) (2012) 204–214.
- [37] Y. Kitajima, T. Ishii, T. Kohda, M. Ishizuka, K. Yamazaki, Y. Nishimura, T. Tanaka, S. Dan, M. Nakajima, Mechanistic study of PpIX accumulation using the JFCR39 cell panel revealed a role for dynamin 2-mediated exocytosis, *Sci. Rep.* 9 (1) (2019) 8666.
- [38] L. Li, Y. Chen, X.B. Wang, X.L. Feng, P. Wang, Q.H. Liu, Comparison of protoporphyrin IX produced cell proliferation inhibition between human breast cancer MCF-7 and MDA-MB-231 cells, *Pharmazie* 69 (8) (2014) 621–628.
- [39] S.J. Chadwick, D. Salah, P.M. Livesey, M. Brust, M. Volk, Singlet oxygen generation by laser irradiation of gold nanoparticles, *J. Phys. Chem. C* 120 (19) (2016) 10647–10657.
- [40] M. Hoogenboom, D. Eikelenboom, M.H. den Brok, A. Heerschap, J.J. Futterer, G. J. Adema, Mechanical high-intensity focused ultrasound destruction of soft tissue: working mechanisms and physiologic effects, *Ultrasound Med. Biol.* 41 (6) (2015) 1500–1517.
- [41] A.E. Fard, A. Zarepour, A. Zarrabi, A. Shanei, H. Salehi, Synergistic effect of the combination of triethylene-glycol modified Fe₃O₄ nanoparticles and ultrasound wave on MCF-7 cells, *J. Magn. Magn. Mater.* 394 (2015) 44–49.
- [42] R.P. Singh, P. Ramarao, Cellular uptake, intracellular trafficking and cytotoxicity of silver nanoparticles, *Toxicol. Lett.* 213 (2) (2012) 249–259.
- [43] J. Weyermann, D. Lochmann, A. Zimmer, A practical note on the use of cytotoxicity assays, *Int. J. Pharm.* 288 (2) (2005) 369–376.